Effect of Uniaxial and Hydrostatic Strain on the Optical Constants and the Electronic Structure of Copper*

ULRICH GERHARDT
The James Franck Institute, The University of Chicago, Chicago, Illinois 60637
(Received 27 December 1967)

The linear response of the optical constants of Cu to a general strain is presented for the range $1.5 \leq \hbar\omega \leq 5.5$ eV. The transitions $X_5 \rightarrow X_4'$ at 4.0 eV and $E_F \rightarrow L_1$ at 4.15 eV are identified. The deformation potentials $\partial(E_F - L_3^{\text{upper}})/\partial e = -(1.1 \pm 0.1)$ eV and $\partial(L_1 - E_F)/\partial e = -(9.6 \pm 1.5)$ eV with $e = \Delta V/V$, and $\partial L_1/\partial e_{yz} = -(72 \pm 12)$ eV with $e_{xy} = e_{yz} = e_{zx}$, $e_{xx} = e_{yy} = e_{zz} = 0$ for $\mathbf{k} \| [111]$ are evaluated from the measurements. They are used to derive the volume coefficients of the Fermi energy, $\partial(\ln E_F)/\partial e = -1.1 \pm 0.3$, and of the position of the d bands, $\partial(\ln E_d)/\partial e = -1.2 \pm 0.5$, with respect to Γ_1. The measurements are consistent with the assumption that direct interband transitions dominate the absorption above 2 eV.

INTRODUCTION

APPLYING a shear strain to a single crystal reduces its symmetry and may split formerly degenerate levels. In optical experiments, the first such splitting was observed accidentally in the investigation of the excitonic absorption of germanium.[1–3] The power of the method was soon recognized; it was used to study the excitonic absorption of other crystals, e.g., CdTe[4] and Cu_2O.[5] The method was first applied to the continuous interband absorption by studying the strain-induced change of the reflectance of Ge and Si.[6,7] Modulation techniques were also used successfully.[8–10] Polycrystalline films of the noble metals were investigated.[11] A preliminary version of the present paper was published elsewhere.[12]

According to the band-structure calculations of Cu,[13,14] direct, **k**-conserving interband transitions are possible for $\hbar\omega > 2$ eV. These lead to a continuous absorption in contrast to the sharp excitonic structure of solids mentioned above. However, the topology and the symmetry of the problem give rise to singularities in the joint density of states,[15–17] which dominate the behavior of semiconductors and insulators in the region of the interband transitions. In metals, the modifications of this structure due to the overlap of the Fermi energy with the electron bands might give even sharper singularities in the absorption.[18]

The basic virtue of the measurements to be discussed here is their ability to distinguish between singularities of different symmetry. The main difficulty in the analysis is that the "symmetry of a singularity" is quite frequently not well defined. For example, a structure in the absorption caused by an M_1 or an M_2 type singularity in the joint density of states is composed of transitions with **k** vectors terminating on the optical energy surfaces $E(\mathbf{k}) = E(M_1)$ and $E(\mathbf{k}) = E(M_2)$, respectively. These surfaces stretch through the Brillouin zone, i.e., there is a whole range of transitions with different **k** vectors which contribute to the observed structure in the absorption. However, if the structure in the absorption is made up of transitions with wave vectors confined to a region close to a symmetry point $\mathbf{k}_s$ in **k** space, the structure will approximately respond to a perturbation as if it were composed of transitions with $\mathbf{k}_s$ only. We will refer to transitions of this kind as strongly localized transitions. Transitions arising from the M_1 and M_2 type singularities mentioned above are only moderately localized around the corresponding saddlepoints, and some transitions connected with singularities caused by the Fermi energy are not localized at all.

The experiments reported here were done with a technique similar to the one used for the alkali halides.[10] They give the linear response of the optical constants to an arbitrary strain for photon energies between 1.5 and 5.5 eV. This information is used to determine the symmetry of strongly and moderately localized transitions; it also reveals which structure in the absorption

* Work supported by the U. S. Air Force Office of Scientific Research, Contract No. AF 49(638)-1653.

[1] S. Zwerdling, B. Lax, L. M. Roth, and K. J. Button, Phys. Rev. **114**, 80 (1959).
[2] G. G. Macfarlane, T. P. McLean, J. E. Quarrington, and V. Roberts, Phys. Rev. Letters **2**, 252 (1959).
[3] W. H. Kleiner and L. M. Roth, Phys. Rev. Letters **2**, 334 (1959).
[4] D. G. Thomas, J. Appl. Phys. **32**, 2298 (1961).
[5] E. F. Gross, A. A. Kaplyanskii, and V. T. Agekyan, Fiz. Tverd. Tela **4**, 2169 (1962) [English transl.: Soviet Phys.—Solid State **4**, 1588 (1961)].
[6] H. R. Philipp, W. C. Dash, and H. Ehrenreich, Phys. Rev. **127**, 762 (1962).
[7] U. Gerhardt, Phys. Letters **9**, 117 (1964); Phys. Rev. Letters **15**, 401 (1965); Phys. Status Solidi **11**, 801 (1965).
[8] W. E. Engeler, H. Fritzsche, M. Garfinkel, and J. J. Tiemann, Phys. Rev. Letters **14**, 1069 (1965); W. E. Engeler, M. Garfinkel, J. J. Tiemann, and H. Fritzsche, *in Colloquium on the Optical Properties and the Electronic Structure of Metals and Alloys, Paris, 1965*, edited by F. Abelès (North-Holland Publishing Co., Amsterdam, 1966), p. 189.
[9] G. W. Gobeli and E. O. Kane, Phys. Rev. Letters **15**, 142 (1965).
[10] U. Gerhardt and E. Mohler, Phys. Status Solidi **18**, K45 (1966).
[11] M. Garfinkel, J. J. Tiemann, and W. E. Engeler, Phys. Rev. **148**, 695 (1966).
[12] U. Gerhardt, D. Beaglehole, and R. Sandrock, Phys. Rev. Letters **19**, 309 (1967).
[13] B. Segall, Phys. Rev. **125**, 109 (1962).
[14] G. A. Burdick, Phys. Rev. **129**, 138 (1963).
[15] L. Van Hove, Phys. Rev. **89**, 1189 (1953).
[16] J. C. Phillips, Phys. Rev. **104**, 1263 (1956).
[17] D. Brust, Phys. Rev. **134**, A1337 (1964).
[18] H. Ehrenreich and H. R. Philipp, Phys. Rev. **128**, 1622 (1962).

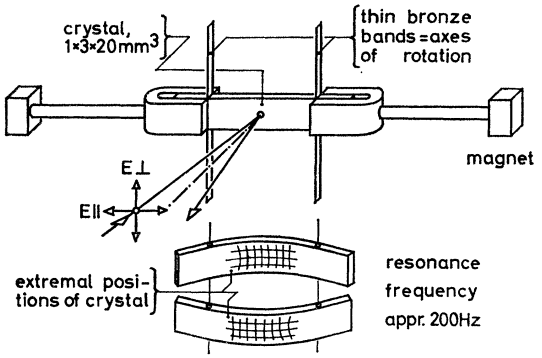

FIG. 1. The mechanical oscillator. The extremal positions of the crystal are shown in the lower half of the figure. The oscillator is driven by an inhomogeneous ac magnetic field which acts on the small permanent magnets at the ends of the level arms.

is due to nonlocalized transitions. In addition, it is used to determine the deformation potentials of the observed transitions. The consistency of the assignment deduced from experiment with the calculated electronic structure of Cu is discussed. The effect of a general strain on the electronic structure is treated theoretically. The results obtained here are compared with those deduced from other experiments (e.g., photoemission[19]) and with theoretical calculations.

EXPERIMENTAL METHOD

Mechanical and Electronic Setup

An ac bending of rectangular single crystalline bars ($1\times3\times20$ mm^3) was used to produce an ac strain at the surface of the crystal. The motion of the crystal is sketched in the lower half of Fig. 1. The two axes of rotation near the ends of the crystal (lower half) are realized by thin bronze bands, soldered to the two clamps which hold the crystal (upper half). Two lever arms are attached to the clamps, carrying small permanent magnets at their ends. The driving forces acting on these magnets were produced by the inhomogeneous ac magnetic field of two electromagnets. The frequency of the current passing through the electromagnets was tuned to the bending mode resonance frequency of the mechanical system.

There are also counterweights attached to the clamps (omitted in Fig. 1 for sake of clarity), which balance the mass of the permanent magnet, the lever arm, and the clamp. After removing the sample, the bronze bands will be a main axis of the moment of inertia for each assembly (magnet, lever arm, clamp, counterweight) individually. Thus, no forces are transmitted through the bronze bands. Otherwise, these forces might give an unwanted wavelength modulation by coupling the mechanical vibration to the monochromator or give acoustical feedback by coupling the vibration to the photomultiplier.

The reflected-light intensity, slightly modulated by the strain-induced change of the reflectance, was detected by a photomultiplier with quartz window (EMI 9558Q, Trialkali). The dc current of the multiplier did not change when the wavelength setting of the monochromator was changed. This was achieved by using an electronic feedback control of the photomultiplier. Thus the ac component of the anode current of the multiplier was proportional to $\Delta R/R$, the relative change of the reflectance. This component was measured as a function of wavelength by means of a phase-sensitive detector and displayed on an x-y recorder. The linearity of the system was checked with a photodiode; the ac to dc ratio was found to be correct to within $\pm3\%$.

Strain Measurement

The strain at the surface of the sample will be the same as that of a closed ring, formed by joining the ends of a previously straight bar with rectangular cross section, as shown in Fig. 2. This is true if the influence of the clamps can be neglected. The cross section of the ring will generally be no longer rectangular. There are two limiting cases for the stress tensor σ and the strain tensor $\mathbf{e}$ at the middle line of the surface of the ring. One limit is approached if the radius ρ_1 and the thickness d of the ring are large and the width b is small. In this case, the stress tensor and the strain tensor take the form

$$\sigma' = \begin{bmatrix} 0 & & \\ & 0 & \\ & & \sigma_{zz'} \end{bmatrix}; \quad \mathbf{e}' = \begin{bmatrix} e_{xx'} & & \\ & e_{yy'} & \\ & & e_{zz'} \end{bmatrix}. \quad (1)$$

We tried to approach this limit in our measurements. The quantitative conditions for the validity of Eqs. (1) were found experimentally by measuring ρ_1 and ρ_2 of bent aluminum bars of various thicknesses and widths. The strain at the middle part of the surface is given by $|e_{zz'}| = d/2\rho_1$ and $|e_{yy'}| = d/2\rho_2$. On the other hand, the ratio $|e_{zz'}/e_{yy'}|$ can be calculated using the stress-strain relation and the form of the stress tensor. Using

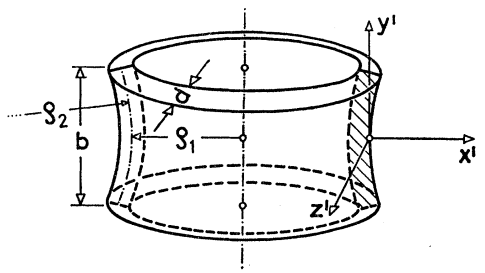

FIG. 2. A closed ring, formed by joining the ends of a previously straight bar with rectangular cross section. The stress axis is z'.

[19] C. N. Berglund and W. E. Spicer, Phys. Rev. **136**, A1030; **136**, A1044 (1964); *Colloquium on the Optical Properties and the Electronic Structure of Metals and Alloys, Pairs, 1965*, edited by F. Abelès (North-Holland Publishing Co., Amsterdam, 1966), pp. 285 and 296.

the stress tensor given by (1), we found the agreement between the measured and calculated ratio to be better than 3%, provided the condition $|e_{zz}'| \leq 4d^2/b^2$ was fulfilled. In the optical measurements on Cu crystals, typical numbers were $|e_{zz}'| = 4\times10^{-4}$, $4d^2/b^2 = 0.4$. Thus the above condition was always met.

In the actual measurements, the crystal forms a small segment of the ring shown in Fig. 2; the distortions produced by the clamps cannot always be neglected. Measurements of ρ_1 and ρ_2 of large aluminum bars clamped at the ends in a way similar to that shown in Fig. 1 were carried out. The difference between the calculated and the measured $|e_{zz}'/e_{yy}'|$ at the midpoint of the sample was again below 3%, provided the free length of the sample (Fig. 1) was at least twice its width. Typical values for the Cu crystals used in the optical experiments are $l = 10$ mm, $b = 3$ mm, i.e., this condition was also fulfilled.

Figure 3 shows the arrangement to determine the component e_{zz}' of the strain tensor by measurement of the focal length of the cylindrical mirror, formed by the bent sample. The sample was oscillating, and the frequency of the stroboscope was tuned close to the resonance frequency of the sample. The distance between the sample and the image of the slit changed periodically with the difference frequency ω(stroboscope)$-\omega$(sample). The amplitude of the strain at the surface is given by

$$e_{zz}' = \Delta a d(2a_0)^{-2}\{1+[1+(\Delta a/a_0)^2]^{1/2}\}^{-1}, \qquad (2)$$

where a_0 is the position of the image for zero strain and Δa is the difference in the position for maximum extension and compression. The accuracy of this method increases with decreasing distance between lens and sample. It was about $\pm5\%$ for the geometry used here. The components e_{xx}', e_{yy}' of the strain tensor are expressed in terms of the measured component e_{zz}' by means of the stress-strain relation using the form (1) of the stress tensor. The elastic constants are taken from Ref. 20. Because of the sample dimensions chosen, the errors in e_{xx}' and e_{yy}' due to deviations from (1) are smaller than 3%. During the optical measurement, the strain amplitude and phase was monitored by a pickup capacitor, consisting of one of the magnets at the ends of the lever arms (Fig. 1), moving against a fixed, insulated piece of sheet metal.

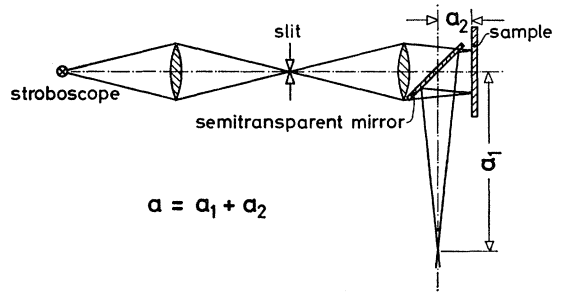

FIG. 3. The optical design which was used to determine the focal length of the cylindrical mirror formed by the bent sample.

[20] *American Institute of Physics Handbook* (McGraw-Hill Book Co., New York, 1957), Chap. 2, p. 56.

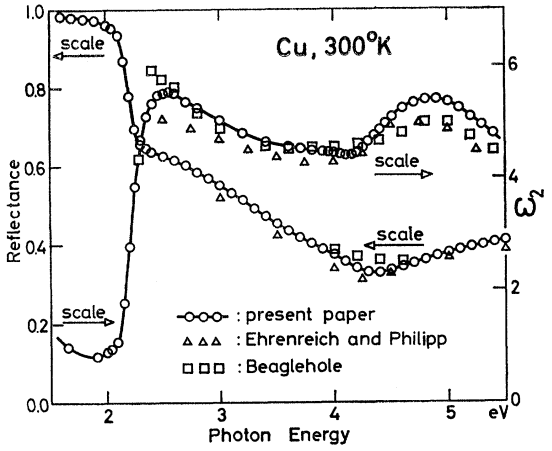

FIG. 4. The reflectance and ϵ_2, the imaginary part of the dielectric constant of Cu at room temperature. The values determined by Ehrenreich and Phillipp (see Ref. 18) and by Beaglehole (see Ref. 22) are only shown if they differ by more than 2% from the values given in the present paper.

Sample Preparation

The orientation of the samples cut from a single crystal was determined to within $\pm1°$ using Laue diagrams. The surface preparation consisted of grinding, mechanically polishing, and electropolishing[21] the sample. The electropolishing was terminated by quickly rinsing in deionized water and alcohol. After taking the sample from the alcohol bath, the thin film of alcohol at the surface was immediately removed by a warm stream of air. The reflectance of a freshly prepared sample, measured within 10 min after the electropolishing, is given in Fig. 4. The growth of an oxide layer at the surface of the sample is responsible for the observed decrease in the reflectance with time. This decrease is most pronounced in the ultraviolet. We observed a 1% decrease at 5.5 eV within 1 h after the electropolishing.

Although the reflectance of our samples was measured in air, it deviates less than 1% from the values determined by Beaglehole,[22] which were measured in a high vacuum after reducing the oxide layer at the surface. The only exception is the region around 4.3 eV. The resolution of the vacuum monochromator used by Beaglehole was not high enough to resolve finer details of the minimum at that energy[23] (see Fig. 4). Thus the oxide layer on our sample modifies the reflectance not more than 1% between 1.5 and 5.5 eV. The reflectance given by Ehrenreich and Philipp[18] is slightly lower

[21] W. J. Tegart, *The Electrolytic and Chemical Polishing of Metals* (Pergamon Press, Inc., New York, 1959), 2nd ed.
[22] D. Beaglehole, Proc. Phys. Soc. (London) 85, 1007 (1965).
[23] D. Beaglehole (private communication).

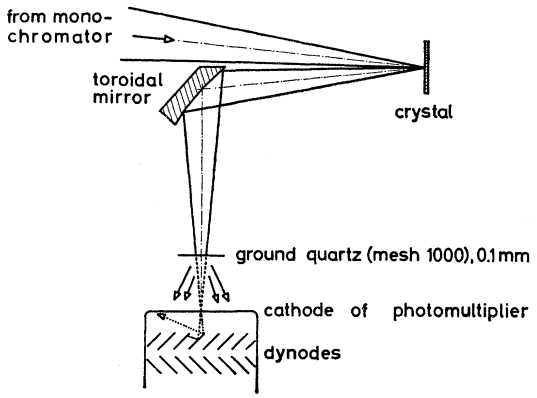

FIG. 5. The optical path of the beam behind the monochromator.

than the one we found, indicating a slightly thicker oxide layer on their sample (Fig. 4).

Figure 4 also contains ϵ_2, the imaginary part of the dielectric constant. It was obtained from a Kramers-Kronig analysis. Between 5.5 and 25 eV, Beaglehole's reflectance values were used. Above 25 eV, the slope of the reflectance was adjusted to reproduce the absolute magnitude of ϵ_2 given by Beaglehole.[22] The slope of the edge in $\epsilon_2(\hbar\omega)$ at 4.3 eV is approximately the same for the function reported here and the one reported by Ehrenreich and Philipp. The edge determined by Beaglehole is somewhat flatter because of the less detailed structure in the reflectance at this energy.

Optical Design and Error Signal

A major difficulty peculiar to modulation techniques such as described here and elsewhere[8,9,11] arises from error signals which might, for example, be generated by the mechanical motion of the crystal. Such an error signal is difficult to separate from the true signal, because both have the same frequency and phase.

In designing the optical path behind the monochromator, we tried to minimize such error signals. One potential source of an unwanted intensity modulation is the large inhomogeneity of the photocathode, which tends to convert small lateral motions of the light beam into intensity modulations. The optical setup is shown in Fig. 5. The beam was focused on the sample and on the semitransparent cathode of the multiplier. The light spot on the cathode is the image of the corresponding point on the sample. It will not change its position, although the reflected beam might sweep over the toroidal mirror because of a motion of the sample or change its solid angle because of a change in the curvature of the sample. However, part of the light is transmitted by the cathode. It will partly reach the cathode again, being scattered by the dynodes. These scattered rays move slightly with respect to the cathode. They were found to be responsible for a substantial error signal, which was strongly wavelength-dependent owing to the wavelength-dependent transmission of the cathode. This error signal was considerably reduced by placing a scattering plate 30 mm in front of the cathode. The plate consisted of a 0.1-mm-thick quartz disk, roughened on both sides with mesh-1000 carborundum. The intensity loss due to this plate was about 40% at 5.5 eV and less at lower energies.

As discussed above, one source of the error signal will be the change of the angle φ between the incident and the reflected beam due to the motion of the sample. This error signal was minimized by shifting the sample perpendicular to the beam in such a way that the beam was reflected at the dynamical center of the sample. In this position φ no longer changes, although the crystal is vibrating (Fig. 1). During this adjustment the error signal itself served to monitor the position of the light spot on the sample with respect to the dynamical center. It was drastically enhanced for that purpose by masking down part of the reflected beam.

In addition to the sources of the error signal discussed above, the small motion of the sample normal to its surface needs to be considered. This will easily produce an intensity modulation if the optical quality of the surface is not excellent. The freshly electropolished surfaces were of high perfection; they did not show any trace of light scattered at the surface. The measurements which will be discussed here were carried out within 2 h after the electropolishing. They contained an error signal of only 2% of the maximum signal. About five days after the electropolishing one could see some weak scattering of light at the surface, probably due to an oxide layer of considerably larger thickness. The error signal was then of the same order of magnitude as the true signal, i.e., it had increased by about a factor of 50, compared to the one immediately after the electropolishing.

The response of the multiplier to small ac magnetic fields (as produced by the driving coils) is another source of error signal. An effective magnetic shielding proved to be essential for the success of our measurements.

Optical Measurements

The reflectance was measured at 4.5° off normal incidence. The difference between near normal and normal incidence reflectance will be neglected in the analysis.

The reflectance of a bent sample contains two contributions. One comes from the discontinuity of ϵ, the complex dielectric constant at the surface. This contribution is identical to that of a sample with homogeneous strain equal to the strain at the surface of the sample. Another contribution is due to the small variation of ϵ, caused by the variation of the strain in the sample in the direction perpendicular to the surface. The second contribution is normally several orders of magnitude smaller than the first one, provided the change of ϵ over one wavelength is small compared to

TABLE I. Definition of the piezo-optical constants.

Strain tensor	Type of strain	Stress axis z'	$\Delta\epsilon_2$ with respect to x', y', z'	Components $\Delta\epsilon_2$ and $\Delta R/R$
$\begin{pmatrix}1&0&0\\0&1&0\\0&0&1\end{pmatrix}e/3$	Hydrostatic	None	$\begin{pmatrix}1&0&0\\0&1&0\\0&0&1\end{pmatrix}\Delta\epsilon_2$	$\Delta\epsilon_2=\frac{1}{3}(W_{11}+2W_{12})e$ $\Delta R/R=\frac{1}{3}(Q_{11}+2Q_{12})e$
$\begin{pmatrix}0&1&1\\1&0&1\\1&1&0\end{pmatrix}e_{yz}$	Trigonal	[111]	$\begin{pmatrix}\Delta\epsilon_2^{\perp}&0&0\\0&\Delta\epsilon_2^{\perp}&0\\0&0&\Delta\epsilon_2^{\parallel}\end{pmatrix}$	$\Delta\epsilon_2^{\parallel}=-2\Delta\epsilon_2^{\perp}=4W_{44}e_{yz}$ $\Delta R/R^{\parallel}=-2\Delta R/R^{\perp}=4Q_{44}e_{yz}$
$\begin{pmatrix}-\frac{1}{2}&0&0\\0&-\frac{1}{2}&0\\0&0&1\end{pmatrix}e_{zz}$	Tetragonal	[001]	$\begin{pmatrix}\Delta\epsilon_2^{\perp}&0&0\\0&\Delta\epsilon_2^{\perp}&0\\0&0&\Delta\epsilon_2^{\parallel}\end{pmatrix}$	$\Delta\epsilon_2^{\parallel}=-2\Delta\epsilon_2^{\perp}=(W_{11}-W_{12})e_{zz}$ $\Delta R/R^{\parallel}=-2\Delta R/R^{\perp}=(Q_{11}-Q_{12})e_{zz}$

the strain-induced change of ϵ at the surface. This condition was always fulfilled in our measurements. The second contribution will be neglected here.

The phase-sensitive detector was locked to the fundamental frequency of the vibration. Thus, only changes of the reflectance proportional to odd powers of strain were detected. Tuning to twice the frequency which should pick up mostly the quadratic effect produced a signal barely above the noise. Thus, only changes linear in the strain components were detected in our measurements.

EXPERIMENTAL RESULTS

Symmetry Relations

The optical properties of a solid are determined by the complex second-rank dielectric tensor $\boldsymbol{\varepsilon}$, which reduces to the unit tensor times the complex dielectric constant for cubic crystals, i.e., cubic crystals are optically isotropic. A general strain applied to these crystals destroys the isotropy. Restricting the discussion to changes linear in the strain components, we may write

$$\Delta\epsilon_{ij}=W_{ijmn}e_{mn}. \tag{3}$$

Cu has the point symmetry O_h. In this case, Eq. (3) parallels the stress-strain relation ($\boldsymbol{\Delta\varepsilon}$ replaces the stress tensor, $\mathbf{W}$ the stiffness tensor), i.e., the fourth-rank piezo-optical tensor $\mathbf{W}$ has three independent complex elements.[8,9,11] We adopt the matrix notation used for the stress-strain relation (see, e.g., Ref. 24). Table I shows the resulting relations for $\boldsymbol{\varepsilon}_2$, the imaginary part of the dielectric tensor. (W_{44} defined in Ref. 11 is four times that of Table I. Using the corresponding definition of the stiffness constant[24] might help to avoid confusion, which frequently arose at that point in the past.) Selecting special geometries, namely the stress axis, the normal to the reflecting plane, and the polarization of the light parallel to the principal axes of $\boldsymbol{\Delta\varepsilon}$ leads to[8,9,11]

$$\Delta R=(\partial R/\partial\epsilon_1)\Delta\epsilon_1+(\partial R/\partial\epsilon_2)\Delta\epsilon_2, \tag{4}$$

where $\Delta\epsilon_1$ and $\Delta\epsilon_2$ are the appropriate eigenvalues of $\boldsymbol{\Delta\varepsilon}_1$ and $\boldsymbol{\Delta\varepsilon}_2$. Thus we can define quantities Q_{ij} (similar to W_{ij}) that describe the relative change of the reflectance. The definition of Q_{ij} is also given in Table I.

[24] C. Kittel, *Introduction to Solid State Physics* (John Wiley & Sons, Inc., New York, 1956), 2nd ed., pp. 87, 89, and 91.

Measurements and Piezo-Optical Constants

Figure 6 contains the measurements of the relative change of the reflectance per strain along the stress axis for three different samples, the stress axes being parallel to [001], [111], and [110], respectively. The surface of the samples was the $(1\bar{1}0)$ plane in all cases. For each stress direction, the reflectance for light polarized parallel and perpendicular to the stress axis is given. The independent information contained in

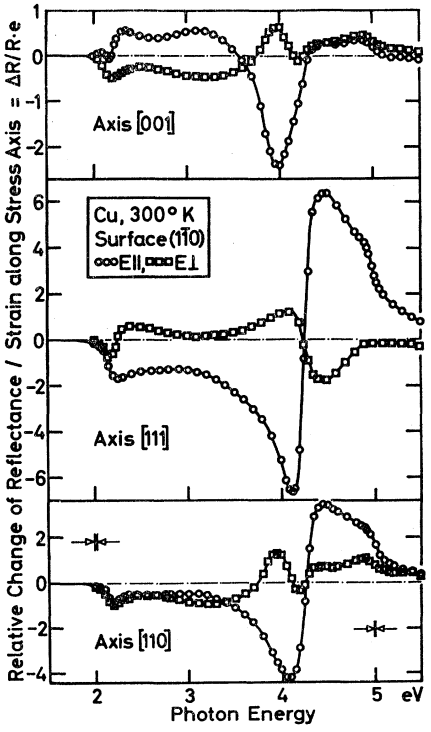

FIG. 6. The relative change of the reflectance per unit strain along the stress axis at room temperature for Cu crystals with the stress axes [001], [111], and [110], and with the reflecting surface $(1\bar{1}0)$. The curves are given for light, plane polarized parallel and perpendicular to the stress axes.

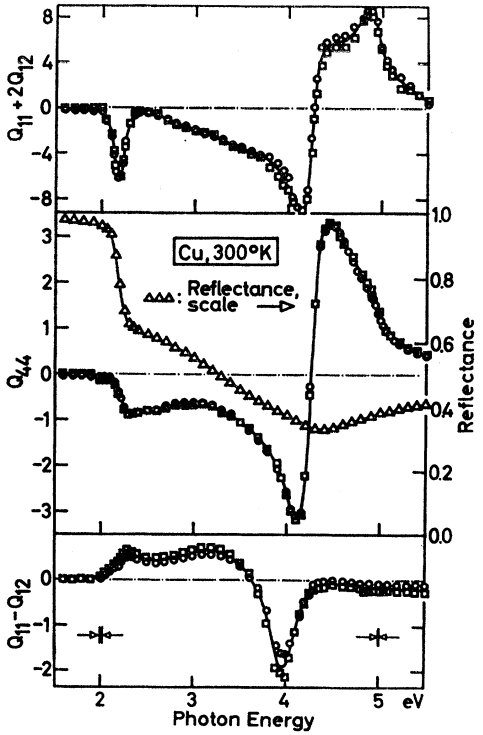

FIG. 7. The relative change of the reflectance of Cu per strain for a change in volume ($Q_{11}+2Q_{12}$) and for trigonal (Q_{44}) and tetragonal ($Q_{11}-Q_{12}$) shear strain, evaluated from the six functions of Fig. 6 as indicated in Table II. The definition of the functions Q_{ij} is given in Table I. The room-temperature reflectance of Cu is also included.

these six measured functions is that of three functions only, e.g., $Q_{11}+2Q_{12}$, Q_{44}, and $Q_{11}-Q_{12}$ as given in Table I. There are in fact two measurements for each of the independent functions. Table II lists the measurements that were used to determine the Q_{ij}; Fig. 7 gives the three functions, together with the reflectance for zero strain. The deviations between points belonging to the same function but originating from different measurements is small; the error signal per strain along the stress axis, estimated from the remaining deviations is approximately ± 0.2. This is about 2% of the maximum signal observed which is $Q_{11}+2Q_{12}=9$ at $\hbar\omega=4.15$ eV.

Figure 8 contains the change of ε_2 resulting from the three independent symmetry distortions, expressed in terms of W_{ij} (see Table I). The function ϵ_2 for zero strain is also included. The quantities W_{ij} were obtained from a Kramers-Kronig analysis of the Q_{ij}. The values for Q_{ij} for $\hbar\omega<1.5$ eV and $\hbar\omega>5.5$ eV are not known. The functions Q_{ij} are zero between 2 and 1.5 eV. The contribution of the free carrier absorption to Q_{ij} remains small further in the infrared.[11] We therefore used $Q_{ij}=0$ as the extrapolation below 1.5 eV. The functions Q_{ij} are small at 5.5 eV, but they are not zero. There are probably nonzero values further in the ultraviolet. In doing the Kramers-Kronig transform, we joined the

TABLE II. Reduction of the measured relative change of the reflectance to the piezo-optical constants Q_{ij}.

Q_{ij}	Determined from	Stress axis	Points in Fig. 7
$Q_{11}+2Q_{12}$	$\Delta R/R^{\parallel}+2\Delta R/R^{\perp}$	[111]	Circles
	$\Delta R/R^{\parallel}+2\Delta R/R^{\perp}$	[001]	Squares
Q_{44}	$\Delta R/R^{\parallel}-\Delta R/R^{\perp}$	[111]	Circles
	$2\Delta R/R^{\parallel}+\Delta R/\Delta^{\perp}$ and $Q_{11}+2Q_{12}$	[110]	Squares
$Q_{11}-Q_{12}$	$\Delta R/R^{\parallel}-\Delta R/R^{\perp}$	[001]	Circles
	$\Delta R/R^{\perp}$ and $Q_{11}+2Q_{12}$	[110]	Squares

functions Q_{ij} smoothly with the zero line for $\hbar\omega>5.5$ eV. In order to evaluate the error introduced by this approximation, another Kramers-Kronig transform was done on $Q_{11}+2Q_{12}$. This time the function was extrapolated to the minimum $Q_{11}+2Q_{12}=-2$ at 6 eV and joined smoothly with the zero line above 6.5 eV. The deviation in $W_{11}+2W_{12}$ for the two extrapolations is 5 at 5.5 eV; this is 6 % of the maximum value (81.5 at 4.3 eV). The weighting function in the Kramers-Kronig integral assures that the error due to the extrapolation decreases with decreasing energy. The error bars near 5.5 eV in Fig. 8 give the deviation due to the extrapolation discussed above, whereas the ones at 3.5 eV give the uncertainty produced by the error signal in $\Delta R/R$.

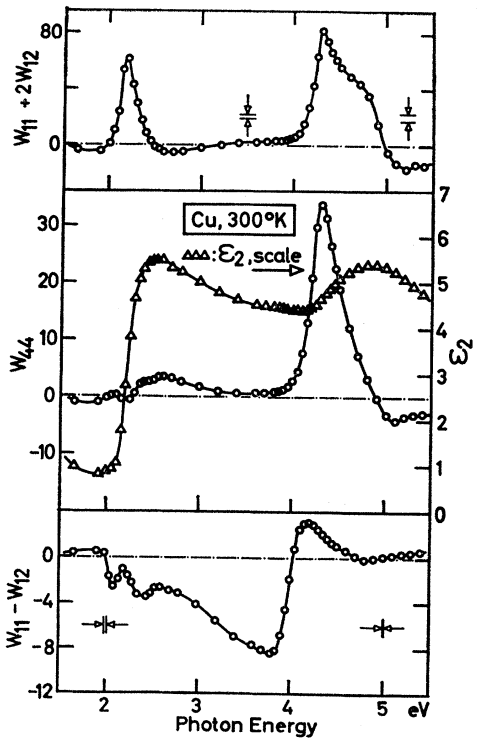

FIG. 8. The change of the imaginary part of the dielectric constant of Cu per strain for a change in volume ($W_{11}+2W_{12}$) and for trigonal (W_{44}) and tetragonal ($W_{11}-W_{12}$) shear strain and the imaginary part of the dielectric constant. The definition of the functions W_{ij} is given in Table I.

TABLE III. Symmetry rules for the optical transitions, considering the splitting of the **k** degeneracy only.

$W_{44}\neq 0$;	$W_{11}-W_{12}=0$	Λ or L transitions
$W_{44}=0$;	$W_{11}-W_{12}\neq 0$	Δ or X transitions
$W_{44}\neq 0$;	$W_{11}-W_{12}\neq 0$	All transitions except Λ, L, Δ, X

The spectral resolution given in Figs. 6–8 is the half-width of atomic mercury lines, as recorded with our optical system.

THEORETICAL ANALYSIS

Symmetry Rules for Optical Transitions

Throughout the theoretical analysis we assume that we are dealing with direct, **k**-conserving interband transitions, i.e., that ϵ_2 is dominated by this process. We exclude the region below 2 eV where free carrier absorption is important.

There are two types of degeneracies in a solid, namely, the orbital degeneracy (e.g., L_3, twofold neglecting spin) and the **k** degeneracy (e.g., the star of $\mathbf{k}_L$ contains four equivalent vectors; any L level will be fourfold degenerate with respect to **k**). Most of the orbital degeneracy is lifted already by spin-orbit interaction. If we include the effect of strain and assume that the center of gravity of the levels under consideration is not changed by the strain, the total splitting will be given by[25]

$$\Delta=(\Delta_{\text{spin orbit}}{}^2+\Delta_{\text{strain}}{}^2)^{1/2}. \tag{5}$$

In Cu, the spin-orbit splitting is about ten times the splitting produced by strain (the strain applied was about 5×10^{-4}). This means that the change of Δ is

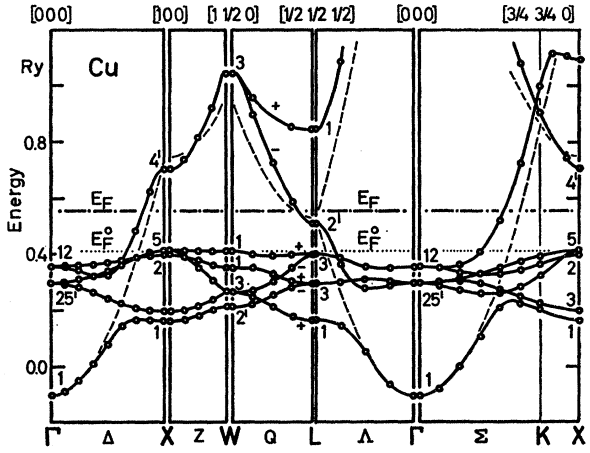

FIG. 9. The band structure of Cu as calculated by Segall (see Ref. 13) and Burdick (see Ref. 14) using Chodorow's potential (see Ref. 26). The dashed curves are the free-electron eigenvalues. E_F is the Fermi energy as calculated by Segall and Burdick and $E_F{}^0$ the Fermi energy calculated for the free-electron eigenvalues of the *sp* bands.

[25] J. Goroff and L. Kleinman, Phys. Rev. 132, 1080 (1963).

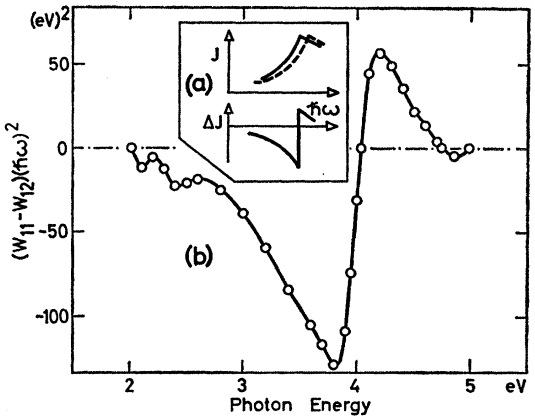

FIG. 10. The insert (a) shows the change of the joint density of states in the neighborhood of an M_1 singularity produced by a rigid energy shift of the joint density of states; in part (b) of the figure the experimental function $(W_{11}-W_{12})(\hbar\omega)^2$ is plotted.

second order in the strain and thus not detected in our measurements. We therefore must exclude the effect of a change of the spin-orbit splitting from our considerations.

Four effects may contribute to the observed $\Delta\epsilon_2$ in Cu, namely, the lifting of the **k** degeneracy, changes in the oscillator strength, changes in the joint density of states, and the splitting of the orbital degeneracy not lifted by spin-orbit interaction. The lifting of the **k** degeneracy normally is the most important effect. We confine the discussion to this effect for the time being. The symmetry rules which follow are summarized in Table III. They were derived by considering the effect of trigonal and tetragonal shear strain on the set of originally equivalent **k** vectors (the star of **k**). These rules depend only on the symmetry of the crystal for zero strain and on the symmetry of the distortion. Exceptions from these rules can arise only from accidental degeneracy, e.g., an L and an X transition at the same energy will produce a nonzero change in ϵ_2 for both trigonal and tetragonal shear strain. It is largely due to these simple symmetry rules that the effect of shear strain on the optical constants is so powerful a method in analyzing the electronic structure of crystals.

Using Table III and the experimental results given in Fig. 8, we expect the edge at 2.1 eV to be caused by nonlocalized transitions, because shear strain gives only very small $\Delta\epsilon_2$ without pronounced symmetry behavior. Going from 2 to 4 eV, a Δ or X transition must become increasingly important. A singularity in the joint density of states connected with these transitions is likely to occur at about 4.0 eV corresponding to the minimum in $W_{11}-W_{12}$ (see Fig. 8). Finally, there must be a pronounced singularity connected with Λ or L transitions at 4.3 eV, which is responsible for the large maximum in W_{44}.

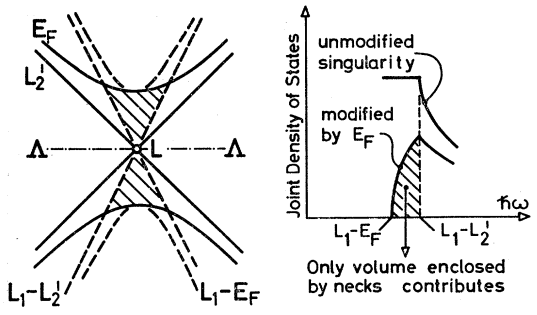

FIG. 11. The energy contours of the surface $E(\mathbf{k})=E_F$, L_2', L_1-L_2', and L_1-E_F around the L point in a plane containing the Λ axis (left-hand part of the figure); the joint density of states near an M_2 singularity and the joint density of states at the same energy, but modified by the Fermi energy (right-hand part).

Comparison Experiment—Band Structure

The energy bands of Cu, as calculated by Segall[13] and Burdick[14] using Chodorow's[26] potential, are shown in Fig. 9. The free-electron eigenvalues are also indicated, together with the Fermi energy for the empty and the actual lattice. We refer to this band structure in the following.

The 2.1-eV edge in ϵ_2 is known to be due to transitions from the top of the d bands to the Fermi surface (FS).[18,27] The experimentally observed energy is well reproduced by the $E(\mathbf{k})$. These transitions will start at Q near L, but at slightly higher energies various parts of the Brillouin zone (BZ) will contribute. This is consistent with the observed lack of response to shear strain.

The only transition at about 4 eV with $\mathbf{k}$ parallel to [001] which is connected with a singularity in the joint density of states is $X_5 \rightarrow X_4'$. The energy difference is 4.0 eV, which is 0.1 eV larger than the position of the minimum in $W_{11}-W_{12}$. The structure at 4.3 eV must be due to transitions near L, since there are no Λ transitions with comparable energies. The FS $\rightarrow L_1$ transition is closest in energy, although the transitions $L_3{}^l \rightarrow$ FS and $L_1{}^d \rightarrow$ FS are also not far removed (the superscripts l=lower and u=upper distinguished the two L_3 levels in the d bands).

Line-Shape Analysis

The $X_5 \rightarrow X_4'$ transition is related to an M_1 critical point (c.p.) in the joint density of states. The contributions at lower energies, originating from $\Delta_5 \rightarrow \Delta_1$, are truncated by the FS below 2.1 eV. The contributions $J_{\Delta X}$ to the total joint density of states J are shown schematically in Fig. 10(a). The change in J produced by a rigid shift in energy is shown in the lower part. For constant matrix elements, J will be proportional to $(\hbar\omega)^2\epsilon_2$.[28] Even for changing matrix elements we expect $(\hbar\omega)^2\epsilon_2$ to follow more closely the actual dependence of J than ϵ_2 itself. Figure 10(b) gives the function $(\hbar\omega)^2(W_{11}-W_{12})$, which is to be compared with the predicted change of Fig. 10(a). The agreement shows that the functional dependence of $W_{11}-W_{12}$ is consistent with that predicted by the above assignment.

Considering the 4.3 eV structure in W_{44}, we may compare ϵ_2 and J directly, because the structure is confined to a narrow energy region. The main difference between the $L^d \rightarrow$ FS (M_1 c.p.) and the FS $\rightarrow L_1$ transitions (M_2 c.p.) is the way the original contributions to the joint density of states are truncated by the FS. In Fig. 11, the lines of constant energy are shown for the L_2' band and for the difference L_1-L_2' in a plane containing the Λ axis. The joint density of states around the M_2 c.p. is modified as shown in Fig. 11. The energy difference $E_N=E_F-L_2'$ is small compared to L_1-L_2' (the symmetry labels such as L_1 are also used to denote the corresponding eigenvalues for typographical convenience). In this case, the variation of J in the region $L_1-E_F \leq \hbar\omega \leq L_1-L_2'$ is given by

$$J(\hbar\omega)=4\pi\Omega(2\pi)^{-3}m_{\parallel}{}^{1/2}m_{\perp}(\hbar\omega-L_1+E_F)^{1/2}. \quad (6)$$

In the derivation of Eq. (6) the neck was approximated by a cylinder. The slope of J as given by Eq. (6) is largest for $\hbar\omega$ slightly larger than L_1-E_F. The slope at $\hbar\omega=L_1-E_F$ will be finite because of lifetime broadening. The largest values of W_{ij} will thus occur at $\hbar\omega$ slightly larger than L_1-E_F, provided W_{ij} is caused by an energy shift of the edge in ϵ_2. Figure 11 and Eq. (6) show that the FS $\rightarrow L_1$ transitions are strongly localized around the L point; all $\mathbf{k}$ vectors terminate in a region enclosed by the neck.

The $\mathbf{k}$ vectors of transitions $L^d \rightarrow$ FS terminate outside the neck, i.e., these transitions are not localized. According to Table III, we expect a change in ϵ_2 for both trigonal and tetragonal shear strain, and we expect this change to be small. The experiments show a very large W_{44}. The small $W_{11}-W_{12}$ at the same energy is probably left from the $X_5 \rightarrow X_4'$ transitions near by (this is the accidental degeneracy mentioned above). Thus the structure at 4.3 eV is most probably due to the strongly localized FS $\rightarrow L_1$ transitions.

The values of the square of the momentum matrix elements M for the transitions of interest here, as calculated by Mueller,[29] are given in Table IV. The oscillator strength for the $L_2' \rightarrow L_1$ transition is much larger than that for transitions originating from d band states. In fact, Mueller and Phillips[29] found that about 40% of the total ϵ_2 around 4.5 eV is due to the conduction-band–conduction-band transitions. The actual value might be somewhat lower due to lifetime broadening, which tends to reduce the height of the sharp structure in ϵ_2, originating from these transitions (Fig.

[26] M. Chodorow, Phys. Rev. 55, 675 (1939); Ph.D. thesis, Massachusets Institute of Technology, 1939 (unpublished).
[27] B. R. Cooper, H. Ehrenreich, and H. R. Philipp, Phys. Rev. 138, A494 (1965).
[28] M. H. Cohen, Phil. Mag. 3, 762 (1958).
[29] F. M. Mueller and J. C. Phillips, Phys. Rev. 157, 600 (1967).

TABLE IV. Transition matrix elements in (Ry) for selected transitions.

Transition[a]	$L_2' \rightarrow L_1$	$L_1^d \rightarrow L_2'$	$L_3^l \rightarrow L_2'$	$X_5 \rightarrow X_4'$
$2P_{ij}^2/m$	3.17	0.533	0.015	0.250

[a] The matrix elements are calculated using the eigenvalues given in Ref. 14 [F. M. Mueller (private communication)].

11). From the experimental ϵ_2 we estimate a total contribution of about 30%, extrapolating the contribution of the background below 4.1 eV to about 4.65 eV. The high percentage of $L_2' \rightarrow L_1$ transitions as calculated from theory is consistent with the pronounced edge in the experimental ϵ_2 and with the large W_{44} as well. This leads again to the conclusion that the observed structure in ϵ^2 and $\Delta\epsilon_2$ at 4.3 eV is caused by the FS $\rightarrow L_1$ transition.

Another striking feature of the functions W_{ij} is the vastly different magnitude of W_{44} and $W_{11}-W_{12}$. The maximum $\Delta\epsilon_2$ observed for trigonal shear strain is nine times the corresponding value for tetragonal shear strain (the amount of the strain being the same). This is partly due to the different degree of localization in **k** space discussed above and partly to the difference in the oscillator strength (Table IV). The small oscillator strength for $X_5 \rightarrow X_4'$ as compared with the one for $L_2' \rightarrow L_1$ suggests that there is no pronounced structure in ϵ_2 around 4.0 eV, and indeed the experimental curve is nearly flat in this region. However, we believe to have resolved a tiny hump in our room-temperature measurements of ϵ_2, as shown in Fig. 12. The reflectance at liquid He temperatures[30] shows a well-resolved structure at about the same energy. The transition does show up clearly as a minimum in $W_{11}-W_{12}$ at room temperature.

The hydrostatic change ($W_{11}+2W_{12}$) and the change with trigonal shear strain (W_{44}) have the same shape between 4 and 4.5 eV. The position of the maximum is 4.3 eV in both cases. This suggests that both effects are due to the FS $\rightarrow L_1$ transition. The two functions differ between 4.5 and 5 eV, where $W_{11}+2W_{12}$ exhibits an additional shoulder around 4.8 eV, whereas W_{44} approaches zero rapidly. This behavior can be explained assuming transitions from the bottom of the d bands to the FS. As in the case of the 2.1-eV edge (where the top of the d bands provides the initial states), these transitions originate from general points of the BZ. This explains the lack of response to shear strain. The transitions will of course change under hydrostatic strain. The situation is equivalent to the one at the 2.1-eV edge, where only hydrostatic strain produces a significant change in ϵ_2.

Experimental Deformation Potentials

The assignment of the structure observed in W_{ij} and ϵ_2 has been established in the preceding sections. This information can be used to calculate the deformation potentials of the corresponding transitions from the experiments, i.e., the difference in the deformation potentials of the final and the initial state. Additional knowledge is required to do so, namely, the slope $d\epsilon_2/d(\hbar\omega)$ of that part of ϵ_2 which is responsible for the observed structure in W_{ij} and the selection rules (required for the shear-strain coefficients only). Furthermore, it must be possible to separate that part of W_{ij} which is due to a change of the energy levels from the ones due to modifications of the transition matrix elements M and of the density of states J.

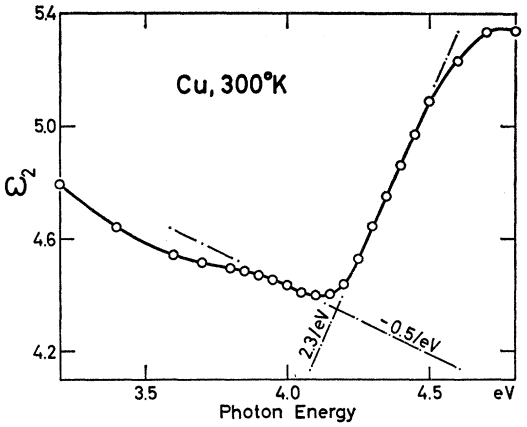

FIG. 12. A blow-up of the imaginary part of the dielectric constant of Cu at room temperature around 4 eV, showing weak structure slightly below 4 eV. The slope of the edge at 4.3 eV and the slope of the background which were used to calculate the deformation potentials of the $E_F \rightarrow L_1$ transition are also included.

The slope of the edge at 2.1 eV is large; modifications due to a background of transitions other than $L_3^u \rightarrow$ FS (e.g., free carrier absorption) will be small. The selection rules are not needed because only hydrostatic strain produces a pronounced change in ϵ_2. The changes in M and J produced by a hydrostatic strain will be much smaller than the ones produced by shear strain, in which case they are required by symmetry.[7] Only $W_{11}+2W_{12}$ is large at this edge, which shows that changes of M and J contribute very little to $W_{11}+2W_{12}$. The deformation potential will be given quite accurately by the maximum value of $W_{11}+2W_{12}$ and by the uncorrected slope of ϵ_2.

As discussed above, the 2.1-eV edge is due to nonlocalized transitions; the transitions with lowest energy have **k** vectors terminating just outside the neck, but at slightly higher energies transitions with **k** vectors located in other parts of the BZ will contribute. The deformation potential determined from the energy shift of the edge will be an average over the deformation potentials of all transitions which contribute. However, the top of the d bands is rather flat, particularly the portion $L_3^u - Q_+$, and it will remain flat if the volume of the crystal is changed. Thus the deformation potentials of transitions contributing to the edge differ only slightly from each other. We therefore no

[30] M. A. Biondi and J. A. Rayne, Phys. Rev. **115**, 1522 (1959).

TABLE V. Matrix elements and strain coefficient of matrix elements which were used to calculate the deformation potentials at L.

Orthogonality matrix element	Tight-binding integrals	Pseudopotential	Hybridization	Zero of d bands above Γ_1
$b_d=-0.366$	$\sigma=-0.332$ eV $\pi=+0.180$ eV $\delta=-0.027$ eV	$V_{111}=0.29$ eV	$H_{\varphi d}=1.32$ eV	$E_d=5.75$ eV
$\partial b_d/\partial e_{yz}=0.73$[a] $k\partial(\ln b_d)/\partial(3k)=0.332$	$R\partial(\ln\sigma)/\partial R=-5.5$[b] $R\partial(\ln\pi)/\partial R=-6.9$ $R\partial(\ln\delta)/\partial R=-8.0$	$\partial V_{111}/\partial e_{yz}=-3.85$ eV[a] $\partial V_{111}/\partial e=-0.93$ eV[c]	d	e

[a] The strain tensor for trigonal distortion is given in Table I. [b] R is the nearest-neighbor distance. [c] $e=\Delta V/V$ is the relative change of the volume
[d] See Text and Figs. 13 and 14. [e] See Table VII.

longer distinguish between the energy shift of the 2.1-eV edge and the change of the $E_F-L_3^u$ separation. The numerical value is $\partial(E_F-L_3^u)/\partial e=-(1.1\pm0.1)$ eV, where $e=\Delta V/V$ denotes the relative change of the volume.

The $X_5\rightarrow X_4'$ transition contributes only a small fraction of the total ϵ_2 at 3.9 eV. It is impossible to get reliable values of $d\epsilon_2/d(\hbar\omega)$ appropriate to this fraction of ϵ_2. We do not attempt to calculate the shear-strain deformation potential of this transition; instead, we simply show that it will produce a negative $W_{11}-W_{12}$ below the energy of the critical point. The level X_4' has free-electron character; it does not interact with the d bands because of symmetry (Fig. 9). Its eigenvalue is k^2 ($\mathbf{k}=\mathbf{X}$, in atomic units), neglecting a small pseudopotential form factor. The shear coefficient for $\mathbf{k}$ perpendicular to z (stress axis, see Table I) is $\partial(\ln k^2)/\partial e_{zz}=+1$. The shear coefficient of the X_5 level, which has tight binding character, will be small compared to that of k^2. Thus the sign of the change in $X_4'-X_5$ is given by the change of k^2. For light polarized parallel to z only those transitions of $X_5\rightarrow X_4'$ with $\mathbf{k}$ perpendicular to z contribute according to the selection rules (these are strictly valid only for the X point and zero spin-orbit splitting, but they will hold approximately). Thus, the M_1 c.p. shifts to higher energies for positive e_{zz}, producing negative values for $W_{11}-W_{12}$ below 4.0 eV, as observed.

The FS$\rightarrow L_1$ transition has been found to be responsible for the large values of W_{44} and $W_{11}+2W_{12}$ at 4.3 eV and for the edge in ϵ_2 at this energy. Because of the strong localization of this transition the deformation potentials derived from W_{ij} will be close to those of the transition with $\mathbf{k}=\mathbf{L}$. Transitions connected with M_1 and M_2 singularities in J which are not modified by the Fermi energy will behave differently, because they are only moderately localized, as discussed in the Introduction. The deformation potentials of transitions with different $\mathbf{k}$ will generally be different. Indeed, Brust and Liu[31] have shown recently that the deformation potential of the transition with $\mathbf{k}$ of the saddlepoint and the energy shift per strain of the corresponding structure in the optical spectrum can differ significantly.

The background slope of ϵ_2 at 4.3 eV due to transitions other than FS$\rightarrow L_1$ cannot be determined rigorously. We use the slope of ϵ_2 at 4.05 eV, which is -0.5/eV (Fig. 12). The similarity of $W_{11}+2W_{12}$ and W_{44} around 4.3 eV shows that changes of M and J which can be large for shear strain only do not contribute significantly to W_{44}. Furthermore, W_{ij} has its maximum where the slope of ϵ_2 is largest and where the contribution of this transition to the total ϵ_2 is still small. If present, changes of J and M would have the largest effect on W_{44} at the maximum contribution of $L_2'\rightarrow L_1$ to ϵ_2. Thus neglecting changes of M and J is justified here. This also justifies the analysis of the previous sections, where we considered the effect of shear strain on the $\mathbf{k}$ degeneracy only.

Without spin, the $L_2'\rightarrow L_1$ selection rules are $M_{z'}\neq0$, $M_{x'}=M_{y'}=0$, where $\mathbf{k}=\mathbf{L}$ is parallel to z' ($z'=$stress axis, Table I). With spin, these rules will still be approximately valid ($|M_{z'}|^2\ll|M_{x'}|^2$). The selection rules for $\mathbf{k}\neq\mathbf{L}$ will be different from the ones given above, even without spin. The strong localization of the transitions in $\mathbf{k}$ space assures that this deviation is small. The shear coefficient of the transition will be calculated neglecting the deviations from the selection rules given above.

The deformation potentials determined from experiment and evaluated using the assumption discussed above are $\partial(L_1-E_F)/\partial e=(-9.6\pm1.5)$ eV and $\partial(L_1-E_F)/\partial e_{yz}=(-72\pm12)$ eV for $\mathbf{k}$ parallel [111]. The largest uncertainty in these coefficients is due to the background slope in ϵ_2 (the values given earlier[12] are 8% higher because the background slope used was -0.3/eV instead of -0.5/eV used here).

Theory of the Deformation Potentials at L

The theoretical estimate of the deformation potentials of the FS$\rightarrow L_1$ transitions given earlier[12] neglected the plane-wave admixture to the wave function of the d state L_{1d}, i.e., d-sp hybridization. The treatment outlined below includes the hybridization.

We use the model Hamiltonian developed by Saffren,[32] Ehrenreich and co-workers,[33] and Mueller[34]

[31] D. Brust and L. Liu, Phys. Rev. **154**, 647 (1967).

[32] M. Saffren, in *The Fermi Surface*, edited by W. A. Harrison and M. B. Webb (John Wiley & Sons, Inc., New York, 1960), p. 341.

[33] L. Hodges and H. Ehrenreich, Phys. Letters **10**, 203 (1965); L. Hodges, H. Ehrenreich, and N. D. Lang, Phys. Rev. **152**, 505 (1966).

[34] F. M. Mueller, Phys. Rev. **153**, 659 (1967).

TABLE VI. Deformation potentials (in eV) of the transitions at L.

Deformation potentials	Experiment: Present paper	Experiment: Zallen[a]	Theory: Present paper	Theory: DFJ[b]	Theory: Jacobs[c]
$\partial(L_1-E_F)/\partial e_{yz}$	-72 ± 12		-56		
$\partial(L_1-E_F)/\partial e$[d]	-9.6 ± 1.5	9.7 ± 2.0		-5.1	
$\partial(E_F-L_3^u)/\partial e$	-1.1 ± 0.1	Absolute value <1.3		-0.8	
$\partial(L_1-L_3^u)/\partial e$				-5.9	-4.1

[a] Reference 47.
[b] Reference 43.
[c] Reference 48.
[d] $e=\Delta V/V$ is the relative change of the volume V.

in the form given by Cohen and Mueller.[35] Using symmetrized plane waves as well as symmetrized tight-binding functions, we can write down the eigenvalues of L_2' and of $L_3^{u,l}$ immediately:

$$L_2'=k^2-V_{111}, \tag{7}$$

$$L_3^{l,u}=E_d+\pi-\delta\pm[(\pi-\delta)^2+4.5(-\sigma+\delta)^2]^{1/2}. \tag{8}$$

The vector $\mathbf{k}$ is that of the L point, V_{111} is a pseudopotential form factor, E_d gives the position of the d bands above Γ_1, and $\sigma\equiv(dd\sigma)$, $\pi\equiv(dd\pi)$, and $\delta\equiv(dd\delta)$ are the two-center tight-binding integrals defined by Slater and Koster.[36] The two L_1 levels are obtained from the secular equation

$$\begin{vmatrix} H_{\Phi\Phi}-E & H_{\Phi d} \\ H_{d\Phi} & H_{dd}-E \end{vmatrix}=0. \tag{9}$$

The function d is a tight-binding Bloch sum symmetrized to L_1 and Φ is a plane wave symmetrized to L_1 and orthogonalized to d,

$$\Phi=(\varphi-b_d d)/C. \tag{10}$$

The abbreviations used in Eq. (10) are

$$\varphi=(2/V)^{1/2}\cos(\mathbf{k}\cdot\mathbf{r}), \tag{11}$$

$$b_d=\langle\varphi|d\rangle, \tag{12}$$

$$C^2=1-b_d^2. \tag{13}$$

The matrix elements of Eq. (9) are

$$H_{dd}=E_d-4(\pi-\delta), \tag{14}$$

$$H_{\Phi d}=(H_{\varphi d}-b_d H_{dd})/C, \tag{15}$$

$$H_{\Phi\Phi}=(k^2+V_{111}+V_{\varphi\varphi}^{(2)}+b_d^2 H_{dd}-2b_d H_{\varphi d})/C^2. \tag{16}$$

We calculated b_d and the tight-binding integrals using the atomic wave function and the atomic potential calculated by Hartree and Hartree[37] and parametrized by Fletcher and Wohlfahrth.[38] The numerical values are given in Table V. The tight binding integrals agree with those calculated by Fletcher and Wohlfahrth. The value of the orthogonalization integral b_d given by Mueller[34] is 16% lower than the one reported here.

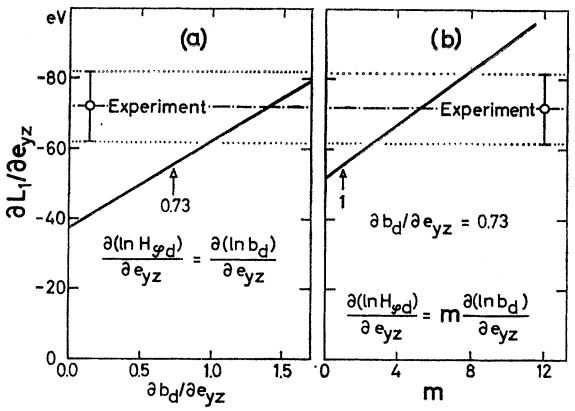

FIG. 13. The dependence of the shear strain deformation potential $\partial L_1/\partial e_{yz}$ on the strain coefficient of the orthogonality integral b_d [part (a) of the figure] and on the strain coefficient of the hybridization $H_{\varphi d}$ [part (b) of the figure]. The value $\partial b_d/\partial e_{yz}=0.73$ was calculated using atomic d functions.

A first-principles calculation of the quantities E_d, $H_{\varphi d}$, and $\Delta V_{\varphi\varphi}^{(2)}$ is extremely difficult and will not be attempted here. Instead, we determine them from the eigenvalues of Fig. 9,[13,14] using the calculated values of b_d and of the tight-binding integrals. In particular, the value of the hybridization integral $H_{\varphi d}$ is evaluated from the difference between H_{dd} (the eigenvalue of L_1^d, neglecting hybridization) and L_1^d. E_d is calculated from $L_3-\Gamma_1$ using Eq. (8). ($L_3^u-L_3^l$ given by this equation agrees with the value taken from Fig. 9. One would expect this, since these bands have no interaction with the sp bands.) The form factor V_{111} given by Eq. (7) is also taken from the calculated band structure.

$\Delta V_{\varphi\varphi}^{(2)}$ is the matrix element of the crystal potential, calculated with the $l=2$ component of φ. It was introduced in the model Hamiltonian[35] following a suggestion by Heine.[39] Its numerical value (calculated using the $L_1-L_1^d$ gap of Fig. 9) is small, namely, -0.75 eV. Neglecting $\Delta V_{\varphi\varphi}^{(2)}$ gives $L_1-L_1^d=9.85$ eV using Eq. (9), which is only 0.60 eV higher than the value of Fig. 9. $\Delta V_{\varphi\varphi}^{(2)}$ will be neglected in the following. The zero-strain values of V_{111}, $H_{\varphi d}$, and E_d are listed in Table V.

The tight-binding parameters for changed nearest-neighbor distances were calculated in the same way as for the distance in the unstrained crystal. For trigonal distortion (Table I) and levels with $\mathbf{k}$ parallel to [111], the strain coefficient of H_{dd} is (R is the nearest-neighbor

[35] M. H. Cohen and F. M. Mueller, in *Atomic and Electronic Structure of Metals* (American Society for Metals, Metals Park, Ohio, 1967), p. 61.
[36] J. C. Slater and G. F. Koster, Phys. Rev. **94**, 1498 (1954).
[37] D. R. Hartree and W. Hartree, Proc. Roy. Soc. (London) **A157**, 490 (1936).
[38] G. C. Fletcher and E. P. Wohlfahrth, Phil. Mag. **42**, 106 (1951).
[39] V. Heine, Phys. Rev. **153**, 673 (1967).

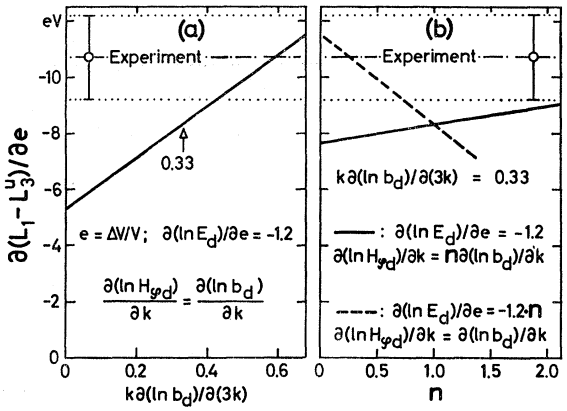

FIG. 14. The dependence of the volume deformation potential $\partial(L_1-L_3^u)/\partial e$ on the strain coefficients of b_d and $H_{\varphi d}$ plotted in a way similar to that of Fig. 13. In addition, the dependence on the volume coefficient of E_d is given [dashed curve in part (b) of the figure].

distance)

$$\partial H_{dd}/\partial e_{yz} = -[12\sigma - 8\pi + 4\delta + R\partial(3\sigma+4\pi+5\delta)/\partial R]. \quad (17)$$

The strain dependence of V_{111} is calculated using a simple model potential.[40] It is constructed from a bare ion potential which is zero inside the core region ($r<r_c$) and equal to the Coulomb potential of a single positive charge outside ($-2/r$ in atomic units). Its Fourier transform is divided by ϵ_q, the static Hartree dielectric function for free electrons,[41] to give the form factor

$$V_q = -8(\cos qr_c)/(\epsilon_q \Omega q^2), \quad (18)$$

where Ω is the volume of the unit cell. The value of r_c (0.23 of the nearest-neighbor distance) is determined by V_{111} of Table V; it is regarded as a constant in calculating the strain coefficients of V_{111} from Eq. (18). The values of the overlap integral b_d for the deformed crystal are calculated in the same way as b_d for zero strain. All strain coefficients discussed above are listed in Table V.

The calculation of the deformation potentials requires additional knowledge, namely, the strain coefficients of $H_{\varphi d}$, E_d, and E_F. The effect of pure trigonal shear strain will be considered first. In this case, there is no change of E_d and E_F linear in the strain components: The center of gravity of originally degenerate levels remains unchanged to first order; this causes E_d and E_F to be constant, too. As a consequence,

$$\partial(L_1-E_F)/\partial e_{yz} = \partial L_1/\partial e_{yz}. \quad (19)$$

A rigorous calculation of $\partial H_{\varphi d}/\partial e_{yz}$ would be even more difficult than the calculation of $H_{\varphi d}$ itself. We therefore simply assume the relative change of b_d and $H_{\varphi d}$ to be identical,

$$\partial(\ln H_{\varphi d})/\partial e_{yz} = \partial(\ln b_d)/\partial e_{yz}. \quad (20)$$

Equation (20) completes the list of strain coefficients which are needed to calculate $\partial L_1/\partial e_{yz}$. Its numerical value (listed in Table VI) is 24% lower than the one determined from the experiments.

Figure 13 illustrates how the theoretical coefficient $\partial L_1/\partial e_{yz}$ changes when changing the assumptions specified above. Figure 13(a) gives the dependence on $\partial b_d/\partial e_{yz}$ assuming Eq. (20) to be valid. Figure 13(b) shows the variation with $\partial(\ln H_{\varphi d})/\partial e_{yz}$ using $\partial b_d/\partial e_{yz} = 0.73$ as calculated from atomic d functions.[37]

Two volume deformation potentials $\partial(E_F-L_3^u)/\partial e$ (determined from the edge at 2.1 eV) and $\partial(L_1-E_F)/\partial e$ (from the edge at 4.3 eV) are used to calculate the volume coefficients of E_d and E_F relative to Γ_1. This can be done more accurately than the large experimental error of the L_1-E_F deformation potential might suggest. Recalling that the error is due to the uncertainty in the appropriate slope of ϵ_2, we note that the relative deviation of the experimental value from the true value is approximately equal for the volume and the shear strain deformation potentials.

Summing the two experimental volume deformation potentials eliminates E_F; the sum $\partial(L_1-L_3^u)/\partial e$ can be used to determine $\partial(\ln E_d)/\partial e$. In doing so, we always treat the normalization factor $\Omega^{-1/2}$ of b_d and $H_{\varphi d}$ explicitly and assume

$$\partial(\ln H_{\varphi d})/\partial k = \partial(\ln b_d)/\partial k, \quad (21)$$

which is the equivalent of Eq. (20). There are several choices on how to proceed. One possibility is to use the coefficient $\partial(\ln b_d)/\partial k$ as calculated with atomic d functions and a value for $\partial(L_1-L_3^u)/\partial e$ which is 24% smaller than the experimental one. Another choice would be to increase $\partial(\ln b_d)/\partial e_{yz}$ until the theoretical value of $\partial L_1/\partial e_{yz}$ matches the experimental one [Fig. 13(a)], to increase $\partial(\ln b_d)/\partial k$ by the same factor, and to use the experimental value of $\partial(L_1-L_3^u)/\partial e$. The volume coefficient of E_d turns out to be the same in both cases, proving that it does not depend drastically on the strain coefficients of b_d and $H_{\varphi d}$. Its numerical value is listed in Table VII. In Fig. 14, $\partial(L_1-L_3^u)/\partial e$ is plotted as a function of the strain coefficients of b_d

TABLE VII. Volume coefficients of the Fermi energy and of the position of the d bands.

Volume coefficients[a]	Present paper	Derived from dHvA[b]	DFJ[c]
$\partial(\ln E_d)/\partial e$	-1.2 ± 0.5		-0.85
$\partial(\ln E_F)/\partial e$	-1.1 ± 0.3	-0.73	-0.86

[a] Γ_1 is the zero of energy and $e=\Delta V/V$ is the relative change of the volume V.
[b] Reference 50.
[c] Reference 43.

[40] N. W. Ashcroft, Phys. Letters **23**, 48 (1966).
[41] W. A. Harrison, in *Frontiers in Physics*, edited by D. Pines (W. A. Benjamin, Inc., New York, 1966), p. 49.

and $H_{\varphi d}$ in a fashion equivalent to that of Fig. 13. The dependence on $\partial(\ln E_d)/\partial e$ is also included [Fig. (14(b)].

In calculating the volume coefficient of E_F, we use the experimental value of $\partial(E_F-L_3{}^u)/\partial e$, the volume coefficient of E_d as calculated above, and Eq. (7), together with the strain coefficients of the tight binding parameters (Table V). The resulting value of $\partial(\ln E_F)/\partial e$ is given in Table VII.

Assuming no strain dependence of b_d and $H_{\varphi d}$ at all (except for $\Omega^{-1/2}$), we find the theoretical values of $\partial L_1/\partial e_{yz}$ and $\partial(L_1-L_3{}^u)/\partial e$ to be 62 and 50% of the corresponding experimental numbers [Eqs. 13(a) and 14(a)], respectively. This part of the deformation potentials is mainly due to the strain dependence of k^2 and, for hydrostatic deformation, to the strain dependence of $\Omega^{-1/2}$.

Discussion

The preceding analysis dealt with the observed structure in W_{ij}. A legitimate question is whether the energy bands predict more structure than actually observed. Pure shear strain will produce a significant change in ϵ_2 only for strongly or moderately localized transitions. Moreover, even if the transitions are localized but have **k** vectors of low symmetry (i.e., neither parallel to [001] nor to [111]), there will be a signal for both trigonal and tetragonal strain (Table III) and the signal will tend to be small. Looking for localized Δ, X, Λ, and L singularities only, we expect the $X_5\rightarrow X_4'$ and the FS $\rightarrow L_1$ transitions to show up between 2 and 5.5 eV, as they do, i.e., the measurements are complete. On the other hand, hydrostatic strain will produce a signal for nonlocalized transitions too. Experimental examples are the maximum in $W_{11}+2W_{12}$ at 2.1 eV and the shoulder at 4.8 eV.

The energies of the identified transitions agree to within ± 0.1 eV with the corresponding difference of the eigenvalues, calculated with Chodorow's[26] potential. Band-structure calculations based on potentials different from that of Chodorow deviate from experiment by as much as 1.5 eV. Table VIII compares the energies of the experimentally observed transitions with predictions of different calculations.[13,14,42–44] There are other experimental results which agree most closely with the result of the $E(\mathbf{k})$ calculation based on Chodorow's potential, the most important of which is the area of the neck, measured with the de Haas–van Alphen effect. The experimental numbers which were re-examined recently[45,46] agree with the calculation[13,14,42] to within 11%. For calculations with other potentials one might not get contact of the Fermi surface with the [111] face of the BZ at all.[42]

TABLE VIII. Energies of observed transitions in eV.

Energy	Experiment	Chodorow[a]	l-dependent[b]	Watson[c]	Self-consistent[d]
$E_F-L_3{}^u$	2.1 $\pm$0.1	2.1	2.3	1.6	3.2
$X_4'-X_5$	4.0 $\pm$0.1	4.0	4.7	3.1	5.5
L_1-E_F	4.15$\pm$0.1	4.0	5.15	3.9	

[a] References 13 and 14.
[b] References 13.
[c] References 42 and 43.
[d] Table II of Ref. 44.

Thus, the experimental evidence for the superiority of the band structure calculated with Chodorow's potential is overwhelming. However, there is no theoretical formalism known today which tells us that we have to choose just this potential. For example, a self-consistent augmented-plane-wave calculation as the one reported by Snow and Waber[44] will agree with the experimental results once the exchange term is properly adjusted, but there is no theoretical justification for such an adjustment.

Zallen[47] measured the change of the reflectance with volume applying hydrostatic pressure directly to the crystal. His results are also listed in Table VI. He could quote only a lower limit for the deformation potential of the 2.1-edge. Our method is much more sensitive here because the large slope of the edge produces a large $\Delta\epsilon_2$ even for the small deformation potential. The two experiments are of comparable accuracy in terms of energy shifts for the 4.3-eV edge. The modulation experiment lost part of its advantage here because the slope is smaller and the slope of the background unknown. The results of the two measurements agree within the experimental error.

Objections might be raised against the procedure used here to calculate the deformation potentials. In particular, one ought to construct the tight-binding functions d from resonance functions rather than from atomic orbitals, as discussed by Heine.[39] However, this would have little effect on the d-sp overlap b_d, because the largest contribution to this integral comes from regions where the resonance function and the atomic d function are identical (the maximum of the integrand lies at 0.53 of the nearest-neighbor distance). The calculated strain coefficients of the tight-binding integrals σ, π, δ (Table V) are higher than predicted by Heine's theory, which would give $R\partial(\ln\beta)/\partial R=-5$ ($\beta=\sigma,\pi,\delta$), but their influence on the deformation potentials is small. Furthermore, it is not clear how the theory of Heine has to be modified if one abandons the muffin-tin approach, i.e., for overlapping potentials.

Two other calculations of the hydrostatic deformation potentials are known.[43,48] Both are listed in

[42] J. S. Faulkner, H. L. Davis, and H. W. Joy, Phys. Rev. **161**, 656 (1967).
[43] H. L. Davis, J. S. Faulkner, and H. W. Joy, Phys. Rev. **167** 601 (1968).
[44] E. C. Snow and J. T. Waber, Phys. Rev. **157**, 570 (1967).
[45] J. P. Jan and M. Templeton, Phys. Rev. **161**, 556 (1967).
[46] W. J. O'Sullivan and J. W. Schriber, Cryogenics **7**, 118 (1967).
[47] R. Zallen, in *Colloquium on the Optical Properties and the Electronic Structure of Metals and Alloys, Paris 1965*, edited by F. Abelès (North-Holland Publishing Co., Amsterdam, 1966), p. 164.
[48] R. Jacobs (private communication).

Table V. The agreement between the measured values and the ones calculated by Davis *et al.*[43] would probably improve if Chodorow's potential were used instead of the one derived from the wave functions given by Watson.[49] The strain coefficients of E_d and E_F given in Ref. 43 are listed in Table VII.

Using the de Haas–van Alphen effect, Templeton[50] measured the change of the neck area with volume and found $\partial(\ln A_n)/\partial e = \frac{2}{3}(4.2\pm 0.2)$. This information can be used to approximately calculate the strain coefficient of E_F. It is determined by Eqs. (7) and (18), neglecting the change of the effective mass of the $L_2'-Q_-$ band. The numerical value of $\partial(\ln E_F)/\partial e$ listed in Table VII is about 34% lower than the one derived from the optical experiments. The agreement will be closer if the change of the effective mass is taken into account: Decreasing the volume ($e>0$) decreases the *d-sp* interaction; the $L_2'-Q_-$ band will get closer to the free-electron parabola (Fig. 9). Thus, including the change of the effective mass, the same change of the neck area requires a larger value of $|\partial(\ln E_F)/\partial e|$.

The $\Delta R/R$ signal measured with strained polycrystalline films[8,11] shows some resemblance to the functional dependence of the hydrostatic effect ($Q_{11}+2Q_{12}$ in Fig. 7), probably with some admixture of the effect produced by trigonal shear strain (Q_{44}). Indeed, one would expect the $\Delta R/R$ signal measured with strained polycrystalline films to be a linear combination of the functions Q_{ij}, provided the signal is due to the change of the reflectance of the material under study. The function $Q_{11}-Q_{12}$ is small for Cu and will therefore contribute but slightly to $\Delta R/R$ measured with polycrystalline films. However, the function $\Delta R/R$ given in Refs. 8 and 11 is not a simple linear combination of $Q_{11}+2Q_{12}$ and Q_{44}. A positive function which increases with energy has to be added to reproduce $\Delta R/R$ as presented in Refs. 8 and 11. The maximum value of this function is of the same order of magnitude as the maximum value in $\Delta R/R$. We believe that this positive function is identical with an error signal produced, e.g., by the mechanical motion of the film. We also found such an error signal, if present, to be strongly energy-dependent. The functions Q_{ij} presented here, which are characteristic of electropolished single crystals have zero values below 2 eV. The signal below 2 eV observed using polycrystalline films[8,11] is probably due to the error signal only.

The FS $\rightarrow L_1$ transition was also identified in the photoemission measurements of Berglund and Spicer.[19] The energy determined from this experiment is identical with the one reported here. The authors introduced the concept of nondirect transitions in the analysis of their data, i.e., transitions which do not conserve **k** directly. The term "indirect transitions" was avoided because the authors wanted to include the possibility that processes different from the usual phonon-assisted transitions are important. The theoretical interpretation of these nondirect transitions is still under discussion (see, e.g., Refs. 51 and 52). Berglund and Spicer concluded from their data that the optical absorption in Cu is dominated by nondirect transitions except for a very small contribution (below 10%) of the direct transitions at L mentioned above.

It is evident from the results presented here that direct transitions must be important. The structure in $W_{11}-W_{12}$ which we identified with the $X_5 \rightarrow X_4'$ transition may serve as an example. One might try to explain it as caused by nondirect transitions starting from various initial states to the same final state X_4'. The **k** degeneracy of X_4' will be lifted by tetragonal shear strain. This might cause the observed $W_{11}-W_{12}$. However, the selection rules for nondirect transitions will generally differ from those for direct transitions. The assumption $|M_x|^2=|M_y|^2=|M_z|^2$ might be adequate for such an averaging process. In this case, there would be no first-order change of ϵ_2 at all, i.e., $W_{11}-W_{12}$ would be zero, in contrast to the experimental result reported here.

The sign (X transition) as well as the magnitude (L transition) of the observed energy shift is consistent with the selection rules for direct transitions. Thus the nondirect transitions must have selection rules identical to those for direct transitions in order to be compatible with our measurements.

The photoemission measurements[19] on Cu can also be explained if one assumes that the absorption above 2 eV is dominated by direct interband transitions.[53] It is more natural to discuss the optical absorption in this region in terms of direct transitions, because this process is well established theoretically and accounts for all details of the experiments persented in this paper.

ACKNOWLEDGMENTS

I should like to thank Professor H. Fritzsche for numerous valuable suggestions and discussions during the course of this research. I am also grateful to Professor D. Beaglehole, Dr. T. Halpern, Dr. F. M. Mueller, and Dr. R. Sandrock for their help and advice.

[49] R. E. Watson, Phys. Rev. **119**, 1934 (1960).
[50] I. M. Templeton, Proc. Roy. Soc. (London) **A292**, 413 (1966).
[51] W. E. Spicer, Phys. Rev. **154**, 385 (1967).
[52] R. K. Nesbet and P. M. Grant, Phys. Rev. Letters **19**, 222 (1967).
[53] U. Gerhardt (to be published).